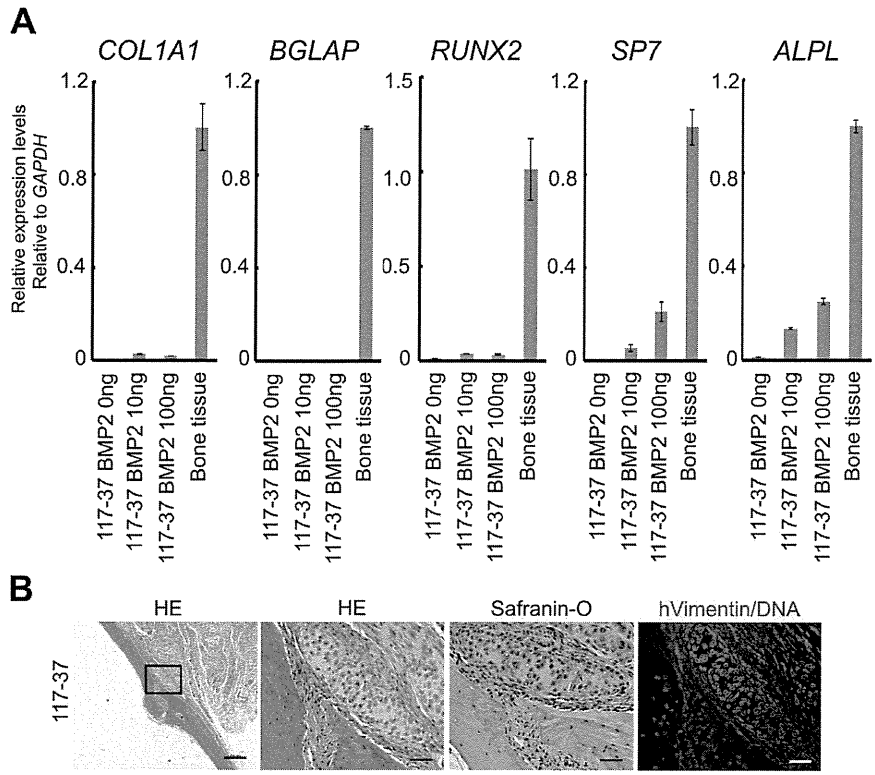

Figure 7. The response of human iChon cells to osteogenic conditions. (**A**) Human iChon cells (line #117-37) were cultured in the osteogenic medium (α-MEM supplemented with 10% FBS, 10 mM β-glycerophosphate, 50 μg/ml ascorbic acid, and 10^{-7} M dexamethasone with the absence or presence of various concentrations of BMP2 as indicated at the bottom of the graphs) for 21 days. RNAs were extracted and subjected to a real-time RT-PCR expression analysis. Error bars indicate the ± SD ($n=3$). (**B**) Human iChon cells were implanted into defects created in the calvaria of SCID mice. Three weeks after implantation, the mice were sacrificed. Semiserial sections were stained with hematoxylin-eosin and safranin O, and immunostained with anti-human vimentin antibodies. The magnification of boxed regions in the left panel is shown in the right three panels, respectively. The bars in the left panels, 250 μm; in the other panels, 50 μm.
doi:10.1371/journal.pone.0077365.g007

not form tumors when transplanted into nude mice, whereas inappropriately reprogrammed mouse induced chondrogenic cells developed into tumors [12]. A possible reason for the more stable karyotypes and non-tumorigenicity of human iChon cells is related to the limited proliferative activities of human iChon cells, whereas mouse induced chondrogenic cells appear to have almost unlimited proliferative potential [12].

Stable karyotypes and non-tumorigenicity are favorable characteristics of human iChon cells when considering their application to regenerative medicine. Although various obstacles remain, human iChon cells can contribute to the development of cell sources to generate hyaline cartilage-related biomaterials.

Supporting Information

Figure S1 The lentiviral *COL11A2*- reporter vector. (A) A schematic representation of the lentiviral vectors carrying EGFP-IRES-Puro linked to the *COL11A2* promoter plus the *COL11A2* enhancer. (B) *Left*, EGFP expression in human dermal fibroblasts (HDFs) and human chondrosarcoma (HCS-2/8) cells transduced with the lentiviral *COL11A2*-reporter vector. Bars, 100 μm. *Right*, the results of a flow cytometric analysis of the EGFP expression from the reporter vectors in the cells.
(JPG)

Figure S2 An immunoblot analysis of the expression of SOX5, SOX6 and SOX9 retroviral vectors in HDF culture. The Plat-E cells were transfected with pMXs-SOX5, pMXs-SOX6, pMXs-SOX9 and pMXs-EGFP. Supernatants containing each of the retroviruses were added to the HDFs that had been nucleofected with Slc7a1. The cells were lysed 7 days after retroviral transduction, and then were subjected to an immunoblot analysis using anti-SOX5, anti-SOX6 and anti-SOX9 antibodies (Supplementary Table S4) as indicated on the left of membranes (top row). Membranes were reprobed with anti-β-actin antibodies (bottom row).
(JPG)

Figure S3 The presence of transgenes in iChon cells, karyotypes of iChon cells, and marker gene expression in iChon cells after passage numbers. (**A**) The presence of transgenes in iChon cells. PCR reactions were performed with template genomic DNA extracted from each iChon cell line using primers specific for each transgene. GAPDH was used as a control. HDF, human dermal fibroblasts. (**B**) The karyotypes of human iChon cells. iChon cell lines #117-3 and #117-37 were examined at passages 18 and 22, respectively. A total of 20 cells for each cell line were examined. (**C**) The results of an analysis of marker gene expression in iChon cell lines (#89-9 and #117-37) after various passage numbers. *P9*, passage 9; *P11*, passage 11; *P13*, passage 13. The expression levels of chondrocyte markers were maintained, and the expression of fibroblast markers was maintained at low levels, after all of the passage numbers examined. Error bars indicate the ± SD (n = 3 dishes). HDFs, human neonatal dermal fibroblasts; HFCs, redifferentiated human fetal chondrocytes.

(JPG)

Figure S4 The frequencies of prechondrogenic cells in HDF cultures. (A) Immunofluorescence staining of human dermal fibroblasts (HDF) in one well of a 6 well plate with anti-SOX9 antibodies. The nuclei were stained with PI. Each whole well was scanned as an 8×8 image, and the tiling images were reconstituted using the Biostation CT (Nikon). Top left, a tiling image of SOX9 immunofluorescence. Bottom left, magnification of the boxed region in the top left panel. Phase images (top right) and nuclear stained images with PI (bottom right) corresponding to the bottom left panel. Bars in the top left panels, 10 mm; bars in the bottom left, top right and bottom right panels, 100 μm. (B) As a positive control for SOX9 immunofluorescence, mouse induced chondrogenic MK-7 cells (Hiramatsu, et al., *J Clin Invest* 121(2): 640-57) were used. Bar, 100 μm. (C) The frequencies of cells showing immunoreactivity against anti-Sox9 antibodies in HDF culture. The cell numbers were counted with the CL-Quant software program (Nikon). Three wells of a 6-well plate were analyzed. The positive cell numbers represent the numbers of cells showing immunofluorescence (Alexa Fluor) with anti-Sox9 antibodies.
(JPG)

Figure S5 Controls for the immunohistochemical analysis. Histological sections from osteochondroma samples dissected at a time of surgery were immunostained with anti-type I collagen and anti-type II collagen antibodies under the conditions used in this study. The hyaline cartilage of the cartilage cap (arrows) showed immunoreactivity against the anti-type II collagen antibody, but did not show immunoreactivity against the anti-type I collagen antibody. Magnification of boxed regions are shown in Figure 4C. Bar, 1 mm.
(JPG)

Table S1 The results of the subcutaneous injection of human iChon cell lines into nude mice.
(DOC)

Table S2 The sequences of the primers used for the transgenes.
(DOC)

Table S3 The sequences of primers for the marker genes, bisulfite sequencing, and PCR cloning.
(DOC)

Table S4 The antibodies used for the experiments.
(DOC)

Movie S1 Time-lapse images taken during the induction of iChon cells. HDFs were transduced with the lentiviral *COL11A2* reporter vector, nucleofected with *Slc7a1*, and transduced with retroviral c-MYC, KLF4 and SOX9 vectors. Cells were replated onto a well of a 6 well plate immediately after completion of the retroviral transduction. The well was cultured in the absence of puromycin and subjected to time-lapse GFP observation using the Biostation CT program (Nikon). Phase (Movie S1) and GFP (Movie S2) images were captured every 8 h for 14 consecutive days. Each image is shown for 0.5 sec, thus 8 h corresponds to 0.5 sec.
(AVI)

Movie S2 Time-lapse images taken during the induction of iChon cells. HDFs were transduced with the lentiviral *COL11A2* reporter vector, nucleofected with *Slc7a1*, and transduced with retroviral c-MYC, KLF4 and SOX9 vectors. Cells were replated onto a well of a 6 well plate immediately after completion of the retroviral transduction. The well was cultured in the absence of puromycin and subjected to time-lapse GFP observation using the Biostation CT program (Nikon). Phase (Movie S1) and GFP (Movie S2) images were captured every 8 h for 14 consecutive days. Each image is shown for 0.5 sec, thus 8 h corresponds to 0.5 sec.
(AVI)

Acknowledgments

We thank Shinya Yamanaka for providing the vectors. We also thank Toshio Kitamura for the Plat-E cells and pMX retroviral vectors. We are thankful to the National BioResource Project - Rat (http://www.anim.med.kyoto-u.ac.jp/NBR/) for providing rat strains (F344-Il2rgtm2kyo). We thank Shigeyuki Wakitani for articular cartilage defect model of rats and Masaharu Takigawa for human chondrosarcoma cells (HCS-2/8). We thank Kunihiko Hiramatsu, Yoshiki Minegishi, Daisuke Ikegami, Takao Iwai Mari Shinkawa and Miho Morioka for their assistance and discussions. We thank Junya Toguchida and Hidetoshi Sakurai for their critical reading of the manuscript.

Author Contributions

Conceived and designed the experiments: HO MO AY HY NT. Performed the experiments: HO MO AY KN NT. Analyzed the data: HO MO KN HY NT. Contributed reagents/materials/analysis tools: HO MO AY KN HY NT. Wrote the paper: HO NT.

References

1. Frisbie DD, Trotter GW, Powers BE, Rodkey WG, Steadman JR, et al. (1999) Arthroscopic subchondral bone plate microfracture technique augments healing of large chondral defects in the radial carpal bone and medial femoral condyle of horses. Vet Surg 28: 242–255.
2. Bae DK, Yoon KH, Song SJ (2006) Cartilage healing after microfracture in osteoarthritic knees. Arthroscopy 22: 367–374.
3. Bedi A, Feeley BT, Williams RJ III (2010) Management of articular cartilage defects of the knee. J Bone Joint Surg Am 92: 994–1009.
4. Goessler UR, Bugert P, Bieback K, Baisch A, Sadick H, et al. (2004) Expression of collagen and fiber-associated proteins in human septal cartilage during in vitro dedifferentiation. Int J Mol Med 14: 1015–1022.
5. Bi W, Deng JM, Zhang Z, Behringer RR, de Crombrugghe B (1999) Sox9 is required for cartilage formation. Nat Genet 22: 85–89.
6. Akiyama H, Chaboissier MC, Martin JF, Schedl A, de Crombrugghe B (2002) The transcription factor Sox9 has essential roles in successive steps of the chondrocyte differentiation pathway and is required for expression of Sox5 and Sox6. Genes Dev 16: 2813–2828.
7. Lefebvre V, Huang W, Harley VR, Goodfellow PN, de Crombrugghe B (1997) SOX9 is a potent activator of the chondrocyte-specific enhancer of the pro alpha1(II) collagen gene. Mol Cell Biol 17: 2336–2346.
8. Lefebvre V, Li P, de Crombrugghe B (1998) A new long form of Sox5 (L-Sox5), Sox6 and Sox9 are coexpressed in chondrogenesis and cooperatively activate the type II collagen gene. EMBO J 17: 5718–5733.
9. Liu Y, Li H, Tanaka K, Tsumaki N, Yamada Y (2000) Identification of an enhancer sequence within the first intron required for cartilage-specific transcription of the alpha2(XI) collagen gene. J Biol Chem 275: 12712–12718.
10. Han Y, Lefebvre V (2008) L-Sox5 and Sox6 drive expression of the aggrecan gene in cartilage by securing binding of Sox9 to a far-upstream enhancer. Mol Cell Biol 28: 4999–5013.
11. Ikeda T, Kamekura S, Mabuchi A, Kou I, Seki S, et al. (2004) The combination of SOX5, SOX6, and SOX9 (the SOX trio) provides signals sufficient for induction of permanent cartilage. Arthritis Rheum 50: 3561–3573.
12. Hiramatsu K, Sasagawa S, Outani H, Nakagawa K, Yoshikawa H, et al. (2011) Generation of hyaline cartilaginous tissue from mouse adult dermal fibroblast culture by defined factors. Journal of Clinical Investigation 121: 640–657.
13. Okita K, Ichisaka T, Yamanaka S (2007) Generation of germline-competent induced pluripotent stem cells. Nature 448: 313–317.
14. Outani H, Okada M, Hiramatsu K, Yoshikawa H, Tsumaki N (2011) Induction of chondrogenic cells from dermal fibroblast culture by defined factors does not involve a pluripotent state. Biochemical and Biophysical Research Communications 411: 607–612.

15. Takahashi K, Tanabe K, Ohnuki M, Narita M, Ichisaka T, et al. (2007) Induction of pluripotent stem cells from adult human fibroblasts by defined factors. Cell 131: 861–872.
16. Tsumaki N, Kimura T, Matsui Y, Nakata K, Ochi T (1996) Separable cis-regulatory elements that contribute to tissue- and site-specific alpha 2(XI) collagen gene expression in the embryonic mouse cartilage. J Cell Biol 134: 1573–1582.
17. Takigawa M, Tajima K, Pan HO, Enomoto M, Kinoshita A, et al. (1989) Establishment of a clonal human chondrosarcoma cell line with cartilage phenotypes. Cancer Res 49: 3996–4002.
18. Takahashi K, Yamanaka S (2006) Induction of pluripotent stem cells from mouse embryonic and adult fibroblast cultures by defined factors. Cell 126: 663–676.
19. Morita S, Kojima T, Kitamura T (2000) Plat-E: an efficient and stable system for transient packaging of retroviruses. Gene Ther 7: 1063–1066.
20. Mashimo T, Takizawa A, Kobayashi J, Kunihiro Y, Yoshimi K, et al. (2012) Generation and characterization of severe combined immunodeficiency rats. Cell Rep 2: 685–694.
21. Argentin G, Cicchetti R, Nicoletti B (1993) Mouse chondrocytes in monolayer culture. In Vitro Cell Dev Biol Anim 29A: 603–606.
22. Akiyama H, Kim JE, Nakashima K, Balmes G, Iwai N, et al. (2005) Osteo-chondroprogenitor cells are derived from Sox9 expressing precursors. Proc Natl Acad Sci U S A 102: 14665–14670.
23. Sridharan R, Tchieu J, Mason MJ, Yachechko R, Kuoy E, et al. (2009) Role of the murine reprogramming factors in the induction of pluripotency. Cell 136: 364–377.
24. Cherry SR, Biniszkiewicz D, van Parijs L, Baltimore D, Jaenisch R (2000) Retroviral expression in embryonic stem cells and hematopoietic stem cells. Mol Cell Biol 20: 7419–7426.
25. Sekiya S, Suzuki A (2011) Direct conversion of mouse fibroblasts to hepatocyte-like cells by defined factors. Nature 475: 390–393.
26. Ieda M, Fu JD, Delgado-Olguin P, Vedantham V, Hayashi Y, et al. (2010) Direct reprogramming of fibroblasts into functional cardiomyocytes by defined factors. Cell 142: 375–386.
27. Pelttari K, Winter A, Steck E, Goetzke K, Hennig T, et al. (2006) Premature induction of hypertrophy during in vitro chondrogenesis of human mesenchymal stem cells correlates with calcification and vascular invasion after ectopic transplantation in SCID mice. Arthritis Rheum 54: 3254–3266.
28. Wernig M, Zhao JP, Pruszak J, Hedlund E, Fu D, et al. (2008) Neurons derived from reprogrammed fibroblasts functionally integrate into the fetal brain and improve symptoms of rats with Parkinson's disease. Proc Natl Acad Sci U S A 105: 5856–5861.
29. Okita K, Matsumura Y, Sato Y, Okada A, Morizane A, et al. (2011) A more efficient method to generate integration-free human iPS cells. Nat Methods 8: 409–412.
30. Seki T, Yuasa S, Oda M, Egashira T, Yae K, et al. (2010) Generation of induced pluripotent stem cells from human terminally differentiated circulating T cells. Cell Stem Cell 7: 11–14.

Biochemical and Biophysical Research Communications 443 (2014) 871–875

Contents lists available at ScienceDirect

Biochemical and Biophysical Research Communications

journal homepage: www.elsevier.com/locate/ybbrc

Methylcobalamin promotes proliferation and migration and inhibits apoptosis of C2C12 cells via the Erk1/2 signaling pathway

Michio Okamoto [a], Hiroyuki Tanaka [a,*], Kiyoshi Okada [a], Yusuke Kuroda [b], Shunsuke Nishimoto [a], Tsuyoshi Murase [a], Hideki Yoshikawa [a]

[a] Department of Orthopaedic Surgery, Osaka University Graduate School of Medicine, 2-2 Yamadaoka, Suita, Osaka 565-0871, Japan
[b] Department of Orthopaedic Surgery, Kansai Rosai Hospital, 3-1-69 Inabaso, Amagasaki, Hyogo 660-8511, Japan

ARTICLE INFO

Article history:
Received 2 December 2013
Available online 14 December 2013

Keywords:
Methylcobalamin
Myoblast
Proliferation
Cell migration
Apoptosis

ABSTRACT

Methylcobalamin (MeCbl) is a vitamin B12 analog that has some positive effects on peripheral nervous disorders. Although some previous studies revealed the effects of MeCbl on neurons, its effect on the muscle, which is the final target of motoneuron axons, remains to be elucidated. This study aimed to determine the effect of MeCbl on the muscle. We found that MeCbl promoted the proliferation and migration of C2C12 myoblasts *in vitro* and that these effects are mediated by the Erk1/2 signaling pathway without affecting the activity of the Akt signaling pathway. We also demonstrated that MeCbl inhibits C2C12 cell apoptosis during differentiation. Our results suggest that MeCbl has beneficial effects on the muscle *in vitro*. MeCbl administration may provide a novel therapeutic approach for muscle injury or degenerating muscle after denervation.

1. Introduction

Vitamin B12 is important for maintaining the normal function of the nervous system, and its deficiency causes a systemic neuropathy called subacute combined degeneration of the spinal cord [1]. Methylcobalamin (MeCbl) is one of the vitamin B12 analogs. We previously reported that MeCbl is the most effective vitamin B12 analog for neurite outgrowth in cerebellar granule neurons and dorsal root ganglion neurons *in vitro* [2] and it increases the mammalian target of rapamycin activity via Akt activation [3]. MeCbl promoted nerve regeneration in *in vivo* nervous disorder models such as those of rat sciatic nerve injury [2,4], streptozotocin-diabetic rats [5], and experimental acrylamide neuropathy [6]. Only one report has described the effect of MeCbl on the neuromuscular junction and indicated that MeCbl promotes the regeneration of motor nerve terminals, a component of the neuromuscular junction, degenerating in the anterior gracile muscle of the gracile axonal dystrophy mutant mouse [4]. Although these previous reports established the effects of MeCbl on neurons and the neuromuscular junction both *in vitro* and *in vivo*, there is no report concerning its effects on the muscle, which is the final target of motoneuron axons. Although MeCbl probably influences not only the nervous system but also the muscle tissue, its effects on the muscle remains unknown.

In the adult skeletal muscle, myogenic satellite cells are quiescent and located between the sarcolemma and basal lamina. In response to stimuli such as myotrauma or nerve injury, myogenic satellite cells become activated, proliferate, and express myogenic markers. Eventually, these cells fuse with existing muscle fibers or fuse together to form new myofibers [7]. Some reports have indicated that transplanting primary satellite cells or injecting fibroblast growth factor-2, which upregulates both myoblast proliferation and fusion, improves the properties of reinnervated skeletal muscles [8,9]. These results suggest that an increase in the number of satellite cells is important as the first step for the regeneration of the damaged skeletal muscle and affects its properties. The Erk1/2 signaling pathway is an important factor involved in myogenic satellite cell proliferation [10,11].

In this study, we demonstrate novel effects of MeCbl on C2C12 myoblasts. We found that MeCbl promotes the proliferation and migration of C2C12 myoblasts via the Erk1/2 signaling pathway. We also exhibited that MeCbl inhibits C2C12 cell apoptosis. Thus, our findings suggest that MeCbl administration may improve the properties of the damaged skeletal muscle or degenerating muscle after denervation.

Abbreviations: MeCbl, Methylcobalamin; GM, Growth medium; DMEM, Dulbecco's modified Eagle's medium; BrdU, 5-Bromo-2-deoxyuridine; DM, Differentiation medium; PI3K, Phosphoinositide 3-kinase.

* Corresponding author. Fax: +81 668793559.
E-mail address: tanahiro-osk@umin.ac.jp (H. Tanaka).

0006-291X/$ - see front matter © 2013 Elsevier Inc. All rights reserved.
http://dx.doi.org/10.1016/j.bbrc.2013.12.056

2. Materials and Methods

2.1. Cell culture

C2C12 myoblasts were cultured under 5% CO_2 at 37 °C in growth medium (GM) consisting of Dulbecco's modified Eagle's medium (DMEM; GIBCO/BRL Life Technologies, Grand Island, NY; not including vitamin B12) supplemented with 10% fetal bovine serum (Gibco/BRL) and 1% penicillin and streptomycin.

2.2. Chemicals and antibodies

MeCbl was purchased from Sigma–Aldrich (St. Louis, MO). An MEK inhibitor, U0126, was purchased from Calbiochem (La Jolla, CA). Anti-p44/42 MAPK (Erk1/2) rabbit monoclonal antibody (1:1000), antiphospho-p44/42 MAPK (Erk1/2) (Thr202/Tyr204) rabbit monoclonal antibody (1:1000), anti-Akt rabbit monoclonal antibody (1:1000), anti-phospho-Akt (Ser473) rabbit monoclonal antibody (1:1000), and anti-β-actin rabbit monoclonal antibody (1:1000) were purchased from Cell Signaling Technology (Beverly, MA). Horseradish peroxidase-conjugated anti-rabbit IgG antibody and ECL reagents were purchased from GE Healthcare (Little Chalfont, UK).

2.3. Immunocytochemistry

C2C12 cells were fixed with 4% paraformaldehyde in PBS for 20 min. After blocking nonspecific binding sites with 5% bovine serum albumin and 0.1% Tween 20 in PBS for 1 h, they were stained with DAPI (Wako Pure Chemical Industries, Osaka, Japan).

2.4. Cell proliferation assay

C2C12 cells were plated at a density of 5×10^3 cells in 6-cm plates and maintained in GM for 24 h prior to stimulation with MeCbl (10–100 μM) or U0126 (10 μM). At 1, 2, 3, and 4 days after the stimulation, they were trypsinized and resuspended. Cell counting was performed in triplicate on separate 10-μl aliquots using a hemacytometer. The proliferative capacity of C2C12 cells was also determined by cell proliferation ELISA using the 5-Bromo-2-deoxyuridine (BrdU) colorimetric system (Roche, Mannheim, Germany) according to the manufacturer's protocol. C2C12 cells were plated at 200 cells/well in a 96-well plate and cultured overnight in GM, followed by stimulation with MeCbl (10–100 μM) or U0126 (10 μM) for 72 h. The cells were labeled with BrdU (10 μM) for 2 h and reacted with anti-BrdU fluorescence-labeled antibody. Absorbance was directly measured using a spectrophotometric microplate reader (Thermo Fisher Scientific, Waltham, MA) at a test wavelength of 450 nm and a reference wavelength of 490 nm. This provided a measure of the degree of cell proliferation, and we termed it the proliferation index.

2.5. Western blotting

C2C12 cells were treated in the presence of MeCbl (10–100 μM) for 5 min with or without 10 μM U0126. They were homogenized with 100 μl of Kaplan buffer [150 mM NaCl, 50 mM Tris–HCl (pH 7.4), 1% NP-40, 10% glycerol, and a protease inhibitor cocktail] and clarified by centrifugation. Each sample including 18 μg of proteins was separated by SDS–PAGE and transferred onto polyvinylidene difluoride membranes. After blocking nonspecific binding sites with a blocking buffer [5% skimmed milk/1% Tween 20 in 20 mM TBS (pH 7.6)] for 1 h, the membranes were incubated overnight at 4 °C with monoclonal primary antibodies. Next, they were incubated with horseradish peroxidase-conjugated anti-rabbit secondary antibody (1:1000) and subjected to ECL reagents. Protein expression levels were determined using the FAS-1000 system (Fuji Photo Film, Tokyo, Japan). Integrated optical densities of immunoreactive protein bands were measured using Scion Image software (Scion Corporation, Frederick, MD). To calculate normalized density, the density of phospho-Erk1/2 or phospho-Akt was divided by that of total Erk1/2 or total Akt, respectively, in the same membrane.

2.6. Wound healing assay

An *in vitro* wound healing assay was performed by the mechanical disruption of confluent monolayers of C2C12 cells as described previously [12]. C2C12 cells were cultured in 6-well plate in GM until they reached confluence. The cell layer was scratched using a scraper to form a continuous, well-delineated area of cellular disruption (4 mm). The cells were then rinsed twice with PBS to remove cellular debris and cultured in GM containing U0126 (10 μM). They were treated with MeCbl (10–100 μM) 1 h after U0126 administration. The medium was changed every other day. Using NIS Elements software (Nikon Instruments Inc, Melville, NY), the distance of the wound at an identical region of the plate was measured. The migration ratio was calculated by dividing the distance of the wound by the initial distance of the wound.

2.7. Apoptosis assay

To induce C2C12 cell differentiation, the cells were grown to approximately 90–100% confluence in GM and the medium was then switched to differentiation medium (DM) consisting of DMEM supplemented with 2% horse serum (Gibco/BRL) in the presence of MeCbl (10–100 μM) with or without U0126 (10 μM) for 3 days. Apoptosis was assessed using the cell death detection ELISA kit (Roche Diagnosis, Mannheim, Germany) according to the manufacturer's instructions. The degree of apoptosis was numerically evaluated by measuring the absorbance. The absorbance of each sample was normalized to that of the control group and designated the normalized absorbance ratio.

2.8. Statistical analysis

Data are expressed as the mean ± SEM. Statistical evaluation was performed by one-way ANOVA and *post hoc* Student's *t*-test.

3. Results

3.1. MeCbl promotes C2C12 cell proliferation via the Erk1/2 signaling pathway

In cases of muscle injury, the subsequent activation and proliferation of myogenic satellite cells are prerequisites for the regeneration of damaged muscle [7]. We focused on the effect of MeCbl on C2C12 cell proliferation. C2C12 cells were cultured with or without MeCbl for 4 days, and the total cell number was then counted every 24 h. Addition of MeCbl at a concentration of 100 μM increased the cell number to 1.29-fold compared with that of the control group ($p < 0.05$, Fig. 1A–D and I). C2C12 cell proliferation was also estimated by the method of BrdU uptake. The proliferation index increased on addition of MeCbl, even at the low concentration of 10 μM ($p < 0.05$, Fig. 1J).

Several intracellular signaling pathways are involved in the proliferation and differentiation of skeletal muscle cells. The activation of the Erk1/2 signaling pathway is known to be associated with myoblast proliferation [11,13], whereas its differentiation is promoted by the activation of the phosphoinositide 3-kinase (PI3K)/

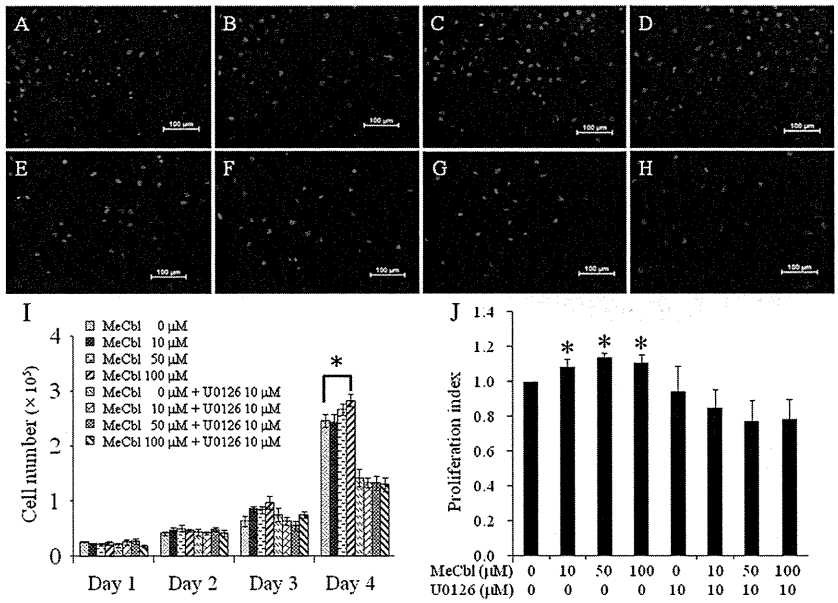

Fig. 1. MeCbl promotes C2C12 cell proliferation via the Erk1/2 signaling pathway. (A–H) Images showing nuclei (DAPI; blue) without MeCbl (A, E) and with MeCbl at 10 μM (B, F), 50 μM (C, G), and 100 μM (D, H). The cells in A–D were treated only with DMSO, and those in E–H were treated with 10 μM U1026. Bars indicate 100 μm. (I) Cell numbers for 4 days after treatment with or without MeCbl (10–100 μM) or U0126 (10 μM). Data are expressed as the mean ± SEM from 3 independent experiments (*$p < 0.05$). (J) Cell proliferation ELISA showing an MeCbl concentration-dependent increase in the absorbance of immunocytochemical staining of C2C12 cells with the proliferation marker BrdU for 72 h. Error bars indicate mean ± SEM. Results are representative of 8 independent experiments (*$p < 0.05$). (For interpretation of the references to color in this figure legend, the reader is referred to the web version of this article.)

Akt pathway [14,15]. To determine whether the signaling pathway plays a role in C2C12 cell proliferation by MeCbl, we estimated the activity of Erk1/2 and Akt by Western blotting. The activity of Erk1/2 increased to 1.49- and 1.44-fold compared with that of the control group 5 min after the addition of MeCbl at the concentration of 50 ($p < 0.05$) and 100 μM ($p < 0.01$), respectively (Fig. 2A). MeCbl did not affect the activity of Akt in C2C12 cells in GM (Fig. 2B). To estimate the duration of upregulated Erk1/2 activity by MeCbl, we observed the Erk activity for 72 h. The activation of the Erk1/2 was not observed 1, 6, 24, 48, and 72 h after the addition of MeCbl (Fig. 2C), whereas MeCbl increased its activity 5 min after the addition (Fig. 2A).

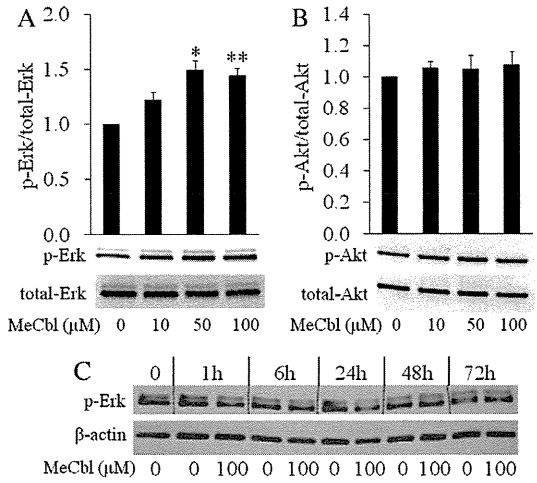

Fig. 2. MeCbl induces Erk1/2 phosphorylation in C2C12 cells C2C12 cells were stimulated with MeCbl for 5 min. Erk1/2 (A) and Akt (B) activities were detected by Western blotting. Quantification of normalized densities for Erk1/2 and Akt activities is shown. MeCbl increased Erk1/2 activity but did not affect Akt activity. Data are expressed as the mean ± SEM from 3 independent experiments (*$p < 0.05$, **$p < 0.01$). (C) The Erk1/2 activity was observed for 72 h after the stimulation with MeCbl. No difference in its activity was observed from 1 to 72 h.

Because the Erk1/2 signaling pathway and not Akt was activated by MeCbl in C2C12 cells in GM, U0126 (a specific Mek/Erk inhibitor) was also added to the proliferation assay in the presence of MeCbl. U0126 abolished C2C12 cell proliferation by MeCbl in terms of the total cell number (Fig. 1E–I) and BrdU uptake (Fig. 1J). These findings suggest that MeCbl accelerates C2C12 cell proliferation via the Erk1/2 signaling pathway.

3.2. C2C12 cell migration is promoted by MeCbl with Erk1/2 activity

The activation of the Erk1/2 signaling pathway is associated with not only proliferation but also migration of C2C12 cells [16]. Thus, we examined the effect of MeCbl on C2C12 cell migration in a wound healing assay. A layer of confluent C2C12 cells was scratched using a cell scraper, and the distance between the cells was measured. The initial distance of the wound did not differ significantly among all the groups (data not shown). On day 4, not day 3, we observed significant differences in the migration ratios between the control and MeCbl groups ($p < 0.05$, Fig. 3A–D and I). The Erk1/2 activity was increased by the addition of MeCbl especially on day 3 (Fig. 3J). The upregulated activity of the Erk1/2 on day 3 might lead to the promotion of the migration ratio on day 4. U0126 inhibited the promotion of the migration ratio on day 4 induced by MeCbl (Fig. 3E–H and I) with the deactivation of the Erk1/2 signaling pathway on day 3 and 4 (Fig. 3J). These results suggest that MeCbl promotes C2C12 cell migration via the Erk1/2 signaling pathway in manner similar to that of proliferation.

3.3. MeCbl inhibits apoptosis during C2C12 cell differentiation via the Erk1/2 signaling pathway

During differentiation *in vitro*, some myoblasts undergo apoptosis, while others withdraw from the cell cycle and form myotubes [17]. We also obtained the higher rate of apoptosis in C2C12 cells cultured in DM than in GM ($p < 0.05$, Fig. 4A). To analyze the role of MeCbl in apoptosis during cell differentiation, C2C12 cells cultured in DM were treated with MeCbl at concentrations of 10–

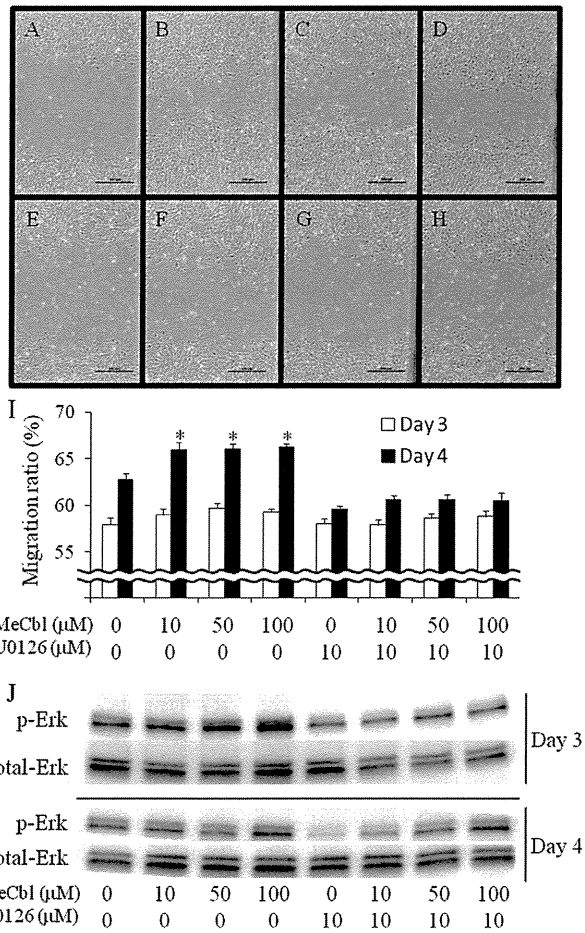

Fig. 3. MeCbl promotes C2C12 cell migration via the Erk1/2 signaling pathway. (A–H) Images of C2C12 cell migration at 4 days after scratching (×200) without MeCbl (A, E) and with MeCbl at 10 μM (B, F), 50 μM (C, G), and 100 μM (D, H). The cells in A–D were treated only with DMSO, and those in E–H were treated with 10 μM U1026. Bars indicate 500 μM. (I) The migration ratio after scratching was quantified on days 3 (white bars) and 4 (black bars). U0126 was added at a concentration of 10 μM. Error bars indicate mean ± SEM. Results are representative of 3 independent experiments (*$p < 0.05$ vs. control). (J) Erk1/2 activity at 3 and 4 days after scratching was detected by Western blotting with or without MeCbl (10–100 μM) or U0126 (10 μM).

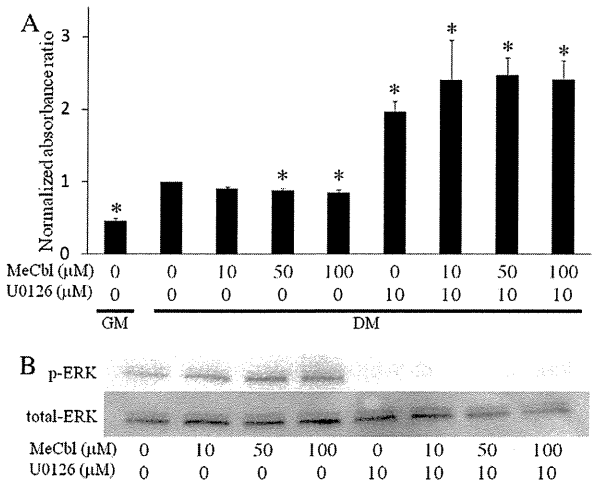

Fig. 4. MeCbl promotes the Erk1/2 activity and inhibits apoptosis during differentiation in C2C12 cell. (A) C2C12 cells were cultured in GM to the almost confluent condition. The medium was then switched to DM with or without MeCbl (10–100 μM) or U0126 (10 μM), and cells were maintained for 3 days. Error bars indicate mean ± SEM. Results are representative of 3 independent experiments (*$p < 0.05$ vs. control in DM). (B) Erk1/2 activity at 3 days after differentiation was detected by Western blotting with or without MeCbl (10–100 μM) or U0126 (10 μM).

100 μM and apoptotic cells were detected. This experiment revealed that the absorbance ratio for apoptotic cells was 12.2% and 14.4% lower in the MeCbl groups at concentrations of 50 and 100 μM, respectively, than that in the control group ($p < 0.05$), although there was no effect in the 10 μM MeCbl group (Fig. 4A). In C2C12 cells, the Erk1/2 signaling pathway plays important roles in not only proliferation and migration but apoptosis [18]. Thus the activation of Erk1/2 signaling pathway was observed during differentiation. MeCbl dose-dependently promoted the activation of Erk1/2 (Fig. 4B). The addition of U0126 increased the apoptotic ratio in the presence or absence of MeCbl (Fig. 4A) with the inactivation of the Erk1/2 (Fig. 4B). These findings suggest that MeCbl inhibits apoptosis during C2C12 cell differentiation with the activation of the Erk1/2 signaling pathway.

4. Discussion

The motor unit in the peripheral nervous system comprises a motoneuron axon terminal, terminal Schwann cell, and muscle. After a motoneuron axon is injured, Wallerian degeneration occurs and the distal part of the injury site degenerates. This mechanism is a prerequisite for the regeneration of motoneuron axons; however, long-term denervation contributes to irreversible changes in the muscle, such as fiber atrophy and fibrosis. In this situation, complete recovery or regeneration of a motor unit cannot be achieved even if the injured axons recover completely, and this results in a serious clinical problem. Preventing degeneration or fibrosis of denervated muscle fibers is very important for regenerating a motor unit in the same manner as axonal regeneration. In this study, we focused on the effects of MeCbl, an analog of vitamin B12, on muscle and found that MeCbl could promote the proliferation and migration of C2C12 cells via the Erk1/2 signaling pathway.

We demonstrated that MeCbl promoted Erk1/2 activation in C2C12 cells (Figs. 2A and 3J). The Erk1/2 signaling pathway is activated in the skeletal muscle in response to physical exercise or injury and plays an important role during myogenesis. Several studies have found that the Erk1/2 signaling pathway promotes proliferation and migration [11,19,20], and our experiments demonstrated that MeCbl promoted the proliferation (Fig. 1) and migration (Fig. 3) of C2C12 cells via the Erk1/2 signaling pathway. However, we found the discrepancies in the duration of the Erk1/2 activation by MeCbl between the cell proliferation assay and the wound healing assay. The activation of Erk1/2 was observed only at the time point of 5 min after the addition of MeCbl, not at 1, 6, 24, 48, 72 h in the cell proliferation assay (Fig. 2A and C), whereas its activity by MeCbl was maintained for several days in the wound healing assay (Fig. 3J). In an *in vitro* wound healing assay using C2C12 cells, phosphorylated Erk1/2 levels reportedly peaked at 10 min after wounding and reached baseline levels at 1 h after wounding [12]. In our experiment, addition of MeCbl maintained phosphorylated Erk1/2 at levels higher than that of the control on days 3 and 4 (Fig. 3J); therefore, the promotion of Erk1/2 activity by MeCbl was not influenced by the phosphorylation of Erk1/2 by mechanical stress induced by scratching monolayer cells in our wound healing assay. We previously reported that MeCbl promoted axonal outgrowth with increased Erk1/2 activity in cerebellar granule neurons and dorsal root ganglion neurons [2]. MeCbl activated Erk1/2 in neurons for 72 h, whereas brain-derived neurotrophic factor activated it for 1 h, suggesting that the mechanisms for activating Erk1/2 differed between MeCbl and neurotrophin like brain-derived neurotrophic factor. The detailed mechanism is unknown, but the activation of Erk1/2 by MeCbl for several days in neurons and in the wound healing assay of C2C12 cells may be maintained by the methylation of some protein kinases [21]. MeCbl may possibly prevent the muscle degeneration or fibrosis

resulting from muscle injury or denervation by promoting axonal outgrowth in neurons and the proliferation and migration of myoblasts accompanied by Erk1/2 activity for long periods.

The PI3K/Akt signaling pathway plays a central role in inhibiting apoptosis [22,23]. In C2C12 cells, Akt plays a protective role in thimerosal-induced apoptosis in GM [24]. Other reports indicated that 17β-estradiol exerts anti-apoptotic effects through the PI3K/Akt signaling pathway in C2C12 cells exposed to hydrogen peroxide [25] and under these conditions Erk2 also plays an important role in the upstream signaling of Akt [18]. Thus, both the Erk and Akt signaling pathways may play important roles in the anti-apoptotic effects in C2C12 cells. We focused on the Erk1/2 signaling pathway in apoptosis during differentiation. The Erk1/2 signaling pathway has reported to be activated in undifferentiated myoblasts and postmitotic myotubes and to be downregulated during the early differentiation stage and its activation is required for optimal differentiation and myotube survival [11]. These facts may support our data that MeCbl promoted the Erk1/2 activation (Fig. 4B) and inhibited the apoptotic rate (Fig. 4A) 3 days after differentiation. Moreover, inactivation of the Erk1/2 pathway by U0126 accelerated the apoptotic rate (Fig. 4A and B). The biphasic activation of the Erk1/2 signaling pathway plays an important role in the proliferation and late stage differentiation in C2C12 cells and MeCbl might have the ability to support its process.

In conclusion, our results indicate that MeCbl promotes the proliferation and migration of C2C12 cells cultured in GM and inhibits apoptosis during differentiation process via the Erk1/2 signaling pathway. We propose that MeCbl may improve muscle injury or prevent muscle degeneration after denervation.

References

[1] G. Scalabrino, B. Monzio-Compagnoni, M.E. Ferioli, E.C. Lorenzini, E. Chiodini, R. Candiani, Subacute combined degeneration and induction of ornithine decarboxylase in spinal cords of totally gastrectomized rats, Lab. Invest 62 (1990) 297–304.

[2] K. Okada, H. Tanaka, K. Temporin, M. Okamoto, Y. Kuroda, H. Moritomo, T. Murase, H. Yoshikawa, Methylcobalamin increases Erk1/2 and Akt activities through the methylation cycle and promotes nerve regeneration in a rat sciatic nerve injury model, Exp. Neurol. 222 (2010) 191–203.

[3] K. Okada, H. Tanaka, K. Temporin, M. Okamoto, Y. Kuroda, H. Moritomo, T. Murase, H. Yoshikawa, Akt/mammalian target of rapamycin signaling pathway regulates neurite outgrowth in cerebellar granule neurons stimulated by methylcobalamin, Neurosci. Lett. 495 (2011) 201–204.

[4] K. Yamazaki, K. Oda, C. Endo, T. Kikuchi, T. Wakabayashi, Methylcobalamin (methyl-B12) promotes regeneration of motor nerve terminals degenerating in anterior gracile muscle of gracile axonal dystrophy (GAD) mutant mouse, Neurosci. Lett. 170 (1994) 195–197.

[5] M. Sonobe, H. Yasuda, I. Hatanaka, M. Terada, M. Yamashita, R. Kikkawa, Y. Shigeta, Methylcobalamin improves nerve conduction in streptozotocin-diabetic rats without affecting sorbitol and myo-inositol contents of sciatic nerve, Horm. Metab. Res. 20 (1988) 717–718.

[6] T. Watanabe, R. Kaji, N. Oka, W. Bara, J. Kimura, Ultra-high dose methylcobalamin promotes nerve regeneration in experimental acrylamide neuropathy, J. Neurol. Sci. 122 (1994) 140–143.

[7] T.J. Hawke, D.J. Garry, Myogenic satellite cells: physiology to molecular biology, J. Appl. Physiol. 91 (2001) 534–551.

[8] Y. Iwata, N. Ozaki, H. Hirata, Y. Sugiura, E. Horii, E. Nakao, M. Tatebe, N. Yazaki, T. Hattori, M. Majima, N. Ishiguro, Fibroblast growth factor-2 enhances functional recovery of reinnervated muscle, Muscle Nerve 34 (2006) 623–630.

[9] C. Lazerges, P.A. Daussin, B. Coulet, R. Boubaker el Andalousi, J.P. Micallef, M. Chammas, Y. Reyne, F. Bacou, Transplantation of primary satellite cells improves properties of reinnervated skeletal muscles, Muscle Nerve 29 (2004) 218–226.

[10] N.C. Jones, Y.V. Fedorov, R.S. Rosenthal, B.B. Olwin, ERK1/2 is required for myoblast proliferation but is dispensable for muscle gene expression and cell fusion, J. Cell Physiol. 186 (2001) 104–115.

[11] Z. Wu, P.J. Woodring, K.S. Bhakta, K. Tamura, F. Wen, J.R. Feramisco, M. Karin, J.Y. Wang, P.L. Puri, P38 and extracellular signal-regulated kinases regulate the myogenic program at multiple steps, Mol. Cell Biol. 20 (2000) 3951–3964.

[12] K. Yeow, C. Cabane, L. Turchi, G. Ponzio, B. Derijard, Increased MAPK signaling during in vitro muscle wounding, Biochem. Biophys. Res. Commun. 293 (2002) 112–119.

[13] D.J. Milasincic, M.R. Calera, S.R. Farmer, P.F. Pilch, Stimulation of C2C12 myoblast growth by basic fibroblast growth factor and insulin-like growth factor 1 can occur via mitogen-activated protein kinase-dependent and -independent pathways, Mol. Cell Biol. 16 (1996) 5964–5973.

[14] Y. Tamir, E. Bengal, Phosphoinositide 3-kinase induces the transcriptional activity of MEF2 proteins during muscle differentiation, J. Biol. Chem. 275 (2000) 34424–34432.

[15] Q. Xu, Z. Wu, The insulin-like growth factor-phosphatidylinositol 3-kinase-Akt signaling pathway regulates myogenin expression in normal myogenic cells but not in rhabdomyosarcoma-derived RD cells, J. Biol. Chem. 275 (2000) 36750–36757.

[16] V. Odemis, K. Boosmann, M.T. Dieterlen, J. Engele, The chemokine SDF1 controls multiple steps of myogenesis through atypical PKCzeta, J. Cell Sci. 120 (2007) 4050–4059.

[17] J. Wang, K. Walsh, Resistance to apoptosis conferred by Cdk inhibitors during myocyte differentiation, Science 273 (1996) 359–361.

[18] A.C. Ronda, A. Vasconsuelo, R. Boland, Extracellular-regulated kinase and p38 mitogen-activated protein kinases are involved in the antiapoptotic action of 17beta-estradiol in skeletal muscle cells, J. Endocrinol. 206 (2010) 235–246.

[19] S.A. Coolican, D.S. Samuel, D.Z. Ewton, F.J. McWade, J.R. Florini, The mitogenic and myogenic actions of insulin-like growth factors utilize distinct signaling pathways, J. Biol. Chem. 272 (1997) 6653–6662.

[20] L. Yahiaoui, D. Gvozdic, G. Danialou, M. Mack, B.J. Petrof, CC family chemokines directly regulate myoblast responses to skeletal muscle injury, J. Physiol. 586 (2008) 3991–4004.

[21] J.I. Toohey, Vitamin B12 and methionine synthesis: a critical review. Is nature's most beautiful cofactor misunderstood?, BioFactors 26 (2006) 45–57

[22] S.G. Kennedy, A.J. Wagner, S.D. Conzen, J. Jordan, A. Bellacosa, P.N. Tsichlis, N. Hay, The PI 3-kinase/Akt signaling pathway delivers an anti-apoptotic signal, Genes Dev. 11 (1997) 701–713.

[23] T.F. Franke, C.P. Hornik, L. Segev, G.A. Shostak, C. Sugimoto, PI3K/Akt and apoptosis: size matters, Oncogene 22 (2003) 8983–8998.

[24] W.X. Li, S.F. Chen, L.P. Chen, G.Y. Yang, J.T. Li, H.Z. Liu, W. Zhu, Thimerosal-induced apoptosis in mouse C2C12 myoblast cells occurs through suppression of the PI3K/Akt/survivin pathway, PLoS One 7 (2012) e49064.

[25] A. Vasconsuelo, L. Milanesi, R. Boland, 17Beta-estradiol abrogates apoptosis in murine skeletal muscle cells through estrogen receptors: role of the phosphatidylinositol 3-kinase/Akt pathway, J. Endocrinol. 196 (2008) 385–397.

整・災外 56：515—524，2013

再生医療の現状と展望：細胞を用いた再生医療

細胞・人工骨複合体移植による骨欠損補填治療法の開発

名井　陽[*1)]　吉川秀樹[*2)]

要旨：大型の骨欠損などの治療困難な病態においては，組織工学・再生医療の技術に大きな期待が寄せられている。われわれは連通多孔体人工骨の骨伝導能と気孔間連通性に着目し，これをscaffoldとして用いて骨髄由来培養間葉系細胞による組織工学・再生医療の研究を行ってきた。2004年から患者骨髄間葉系細胞を用いた骨再生の臨床研究を実施し，安全性と有効性とも，おおむね満足できる結果を得ている。このような幹細胞を使用した再生医療は，コスト，品質管理，安全性，有効性，他の治療法に対する優位性など種々の未解決の課題を抱えており，慎重に，科学的に，かつ迅速に評価し明らかにしていくことが重要である。海外では既に細胞を使った骨再生医療製品が利用されており，わが国でも遅滞なく実用化するために産官学が一体となった研究開発の推進が望まれる。

はじめに

骨には優れた自然治癒能力，再生能力が備わっていると考えられているが，骨腫瘍切除後や重度外傷，骨髄炎，血行不良，偽関節，人工関節の緩みなど，骨形成が不良な状態や，ある程度の大きさの骨欠損が生じた場合には，固定するだけでは必ずしも良好な治癒が得られない。このような難治性骨欠損に対しては，古くから自家骨移植が標準的治療であったが，自家骨の採取手技は侵襲や合併症が多く，使用できる移植骨の量には限界があることから，各種の骨補填材が考案され利用されている。米国では骨バンクが発達しアクセスが容易であることから同種骨が普及しているが，わが国では合成リン酸カルシウムセラミックスの人工骨が1980年頃に世界に先駆けて臨床応用され，広く利用されている。しかしセラミックス人工骨は直接，骨組織と結合することができる「骨伝導能」は有していても，異所性に骨を形成する能力「骨誘導能」はなく，臨床的位置づけとしては標準である自家骨に比べるとまだ劣るという印象である。同種骨は病原伝搬性や拒絶の問題もある。また悪性骨腫瘍切除後の大型骨欠損では腫瘍用人工関節での再建が標準的治療であるが，患者QOLを考慮すると耐久性や機能面で決して満足できる方法とはいえない。

[*1)] Akira MYOUI，大阪大学医学部附属病院未来医療開発部，未来医療センター
[*2)] Hideki YOSHIKAWA，大阪大学大学院医学系研究科，器官制御外科学（整形外科）

Tissue-engineered approach for the treatment of bone defect using mesenchymal cells combined with ceramic bone substitute

Key words：Tissue engineering, Mesenchymal stem cell, Bone substitute

このような背景から，Langer, Vacanti らによって提唱された組織工学（tissue engineering）の概念が普及し再生医療が脚光を浴び始めるようになると，整形外科，歯科の医師や硬組織に関わる研究者らは，再生医療によって人工骨に骨誘導能を賦与することで自家骨と同等かそれ以上の骨欠損修復法を創出することを目指して，実用化に向けた研究を進めてきた。本稿ではわれわれが進めてきた細胞導入人工骨による骨再生についての臨床試験の経験を中心に，骨再生医療の実用化の現状について解説する。

Ⅰ．骨再生のコンセプトと使用する細胞

自家骨移植は患者自身の正常部分の“生きた骨”を採取し，病変部の骨欠損に移植する。そのため拒絶反応もなく移植片そのものが骨芽細胞などの骨形成細胞を含んでおり，また骨形成に関与する生理活性物質が骨基質内に温存されているため，臨床での難治性骨欠損の修復においては同種骨や人工骨に比べ信頼性が高い。この自家骨をしのぐ治療方法を目指して，骨形成細胞が持つ骨誘導能を組織工学的な手法を用いてより強力に作用させ，難治性骨欠損をより確実に修復しようと研究が進められている。これが細胞を用いた骨再生医療である。1990 年代に提唱された組織工学の概念では，細胞，足場（scaffold），調節因子の 3 要素に着目し，これらの適切な組み合わせを用いることにより目的とする組織の再生を目指すというコンセプトとなっているが，骨の組織工学において“細胞”は主として間葉系幹細胞が利用されており，“足場”としてはコラーゲンスポンジ，セラミックス製多孔質人工骨[1)~6)]，セラミックス製人工関節の多孔質表面などが用いられる。

骨の再生医療では倫理的側面や腫瘍化などの問題が実用化に向けた障壁となっている胎児性幹細胞（ES 細胞：embryonic stem cell）や人工多能性幹細胞（iPS 細胞：induced pluripotent stem cell）などの万能細胞ではなく，これらの問題が少ない組織幹細胞，特に間葉系幹細胞あるいはこれに骨芽細胞分化誘導をかけた細胞が用いられている。間葉系幹細胞は，1960 年代に Friedenstein らによって骨髄中の存在が示唆されているが，多分化能と増殖能を併せ持ついわゆる組織幹細胞としてその概念が確立したのは 1990 年代である。骨髄液中には約 0.01～0.1％の割合で間葉系幹細胞が存在すると言われており，接着性の紡錘形～多角形の単核細胞である。細胞表面マーカーとしては，国際細胞治療学会が 2006 年に出したヒト間葉系幹細胞の定義では，CD105，CD73，CD90 が陽性で，CD45，CD34，CD14 または CD11b，CD79a または CD19，HLA-DR が陰性であることとされている[7)]。間葉系幹細胞は，骨髄以外にも脂肪，滑膜など種々の間葉系組織に存在し，分化誘導に関しては骨，軟骨，脂肪など間葉系の組織だけでなく神経などにも誘導可能であることが示されているが，由来組織によって分化誘導の難易度は異なることも知られており，骨芽細胞への分化誘導には骨髄由来の間葉系幹細胞が適していると考えられている。骨髄液からの間葉系幹細胞の分離・増幅は，有核細胞を比較的低濃度で培養することによってコロニー形成してくる細胞（CFU-F）を増幅することで可能である。しかしこの方法で得られる細胞集団における間葉系幹細胞の純度は通常 90％程度にとどまるようである。

細胞のドナーとしては，間葉系幹細胞などの組織幹細胞においても，自家細胞と同種細胞の両方が考えられる。わが国における骨再生の臨床研究は主として免疫原性，病原伝搬性の問題がない自家間葉系幹細胞が用いられることが多いが，間葉系幹細胞は免疫原性が低いと考えられており同種間葉系幹細胞も米国の細胞治療製品や遺伝性疾患の治療を目的とした研究では利用されている。

Ⅱ．セラミックス人工骨 scaffold と骨再生実験（図 1）

ハイドロキシアパタイトや，リン酸 3 カルシウムなどリン酸カルシウム系の多孔体セラミックス人工骨は骨伝導能を有しており，骨組織との親和性が高く，臨床的にも安全性・有効性が確認され，信頼性の高い材料である。特に連通多孔体構造を持つ材料の場合，内部の気孔にまで細胞などを導入することが容易であり，また形状賦与や手術で

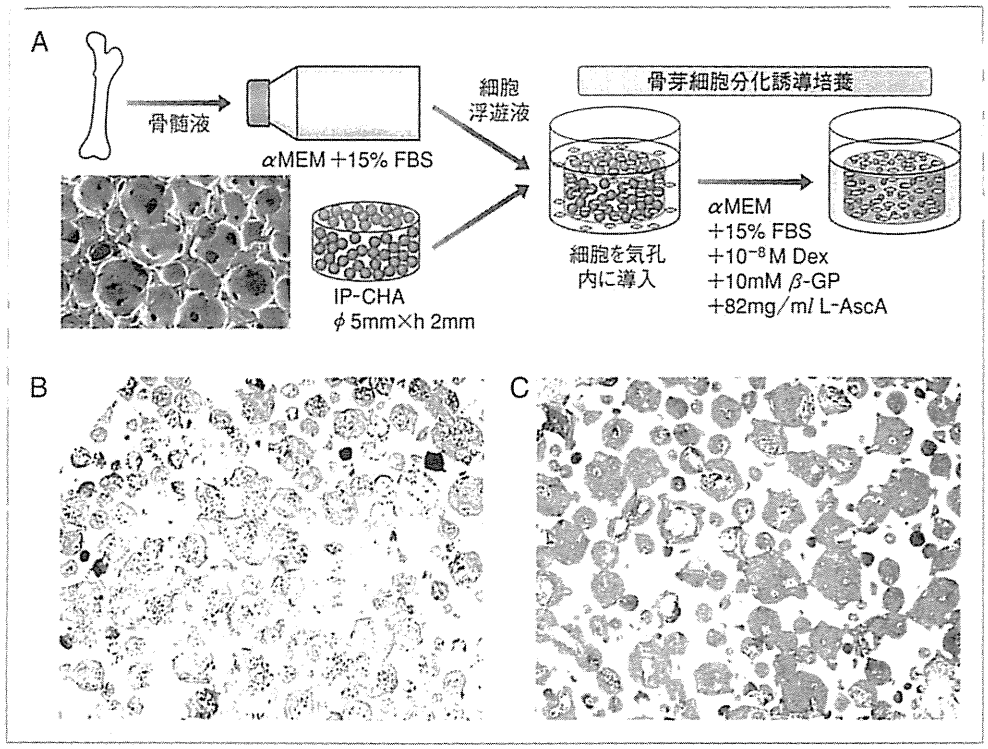

図 1　細胞/セラミックス人工骨複合体による骨再生の実験

A　ラット大腿骨骨髄より得た骨髄細胞を 15%仔牛血清を含む α-MEM 培地で培養し間葉系幹細胞を増幅させる。この細胞の浮遊液に，IP-CHA の円盤状ブロック（φ5 mm×h 2 mm）を浸漬し気孔内に細胞を導入する。さらに 2 週間，L-アスコルビン酸（Asc A），β-グリセロリン酸（GP），デキサメサゾン（Dex）を添加した培地で骨芽細胞への分化誘導培養を行う。

B・C　ラット背部皮下移植後の組織像。移植後 4 週（B）で既に一部の気孔内の骨形成がみられ，移植後 8 週（C）ではほとんどすべての気孔内に良好な骨形成が認められた。

の取り扱いが可能となる程度の強度を有することから，骨再生医療に有用な scaffold として活用できるのではないかと考えられている。これまで間葉系幹細胞と高気孔率，高連通性セラミックス人工骨を足場として利用した動物実験は，われわれの報告を含め多数報告されており，その有用性が確認されている[8)~11)]。われわれは物質材料研究機構，コバレントマテリアル（株），（株）エム・エム・ティーと共同で開発した連通多孔体ハイドロキシアパタイト人工骨（IP-CHA，NEOBONE™）を scaffold として使用し，上述した方法を用いて増幅した間葉系幹細胞を導入して骨芽細胞へ分化誘導したセラミックス人工骨/骨芽細胞複合体を用いた骨再生の研究を進めてきた[12)]。IP-CHA は骨伝導能を有するハイドロキシアパタイト製人工骨で，75%程度の高い気孔率と φ40 μm 程度の気孔間連通孔で互いに連通する φ100～200 μm の球形の気孔を特徴とし，気孔間連通孔を通じて細胞浮遊液の気孔内への導入が容易である。ラット大腿骨骨髄より得た骨髄細胞を，15%仔牛血清を含む α-MEM 培地で 10 日間ほど培養すると，紡錘形の付着性細胞が増殖してくる。この細胞は約 90%が増殖能と骨芽細胞など間葉系細胞への分化能を維持する間葉系幹細胞である。この細胞の浮遊液に，IP-CHA の円盤状ブロック（φ5 mm×h 2 mm）を一晩浸すと IP-CHA の気孔内に細胞が

導入され気孔壁に付着する。これをさらに2週間，アスコルビン酸，β-グリセロリン酸，デキサメサゾンを添加した培地で培養したのち，ラット背部皮下に移植すると，移植後8週でほとんどすべての気孔内に良好な骨形成が認められた[8]。また，同様の手技が可能であることをウサギ前腕橈骨骨幹部欠損モデルでも確認した。これらの結果を踏まえて，われわれは大阪大学医学部附属病院未来医療センターの細胞培養調整施設（cell processing center；CPC）を利用し，良性骨腫瘍および骨腫瘍類似疾患の患者を対象に，「自家骨髄由来培養細胞導入人工骨による骨疾患の治療—第Ⅰ/Ⅱ相臨床試験」を実施した[1]。

Ⅲ．セラミックス人工骨と骨髄由来間葉系幹細胞を用いた臨床研究の実際

「自家骨髄由来培養細胞導入人工骨による骨疾患の治療—第Ⅰ/Ⅱ相臨床試験」の対象は，大阪大学医学部附属病院整形外科を受診した良性骨腫瘍または骨腫瘍類似疾患の患者で，腫瘍を切除後，準備した細胞搭載人工骨を骨欠損部に充填し，術後48週まで定期的経過観察を行った。

1．培養細胞搭載人工骨（培養骨）の作成（図2）

1）治療計画

三次元CT，MRI等の画像診断データで評価した骨欠損の大きさ，形状，骨皮質の欠損状況などに応じて，作成する培養骨の形状（顆粒状か，成形ブロック体か），サイズおよび量を決定し，必要な多孔体人工骨を準備する。

2）血清と骨髄液の採取

自己血貯血に準じて患者から必要量（200～400 m*l*）の末梢血を採取して自己血清を得る。骨髄液の採取は原則として外来処置にて行っている。局所麻酔下に両側の上後腸骨棘付近で骨髄穿刺を行

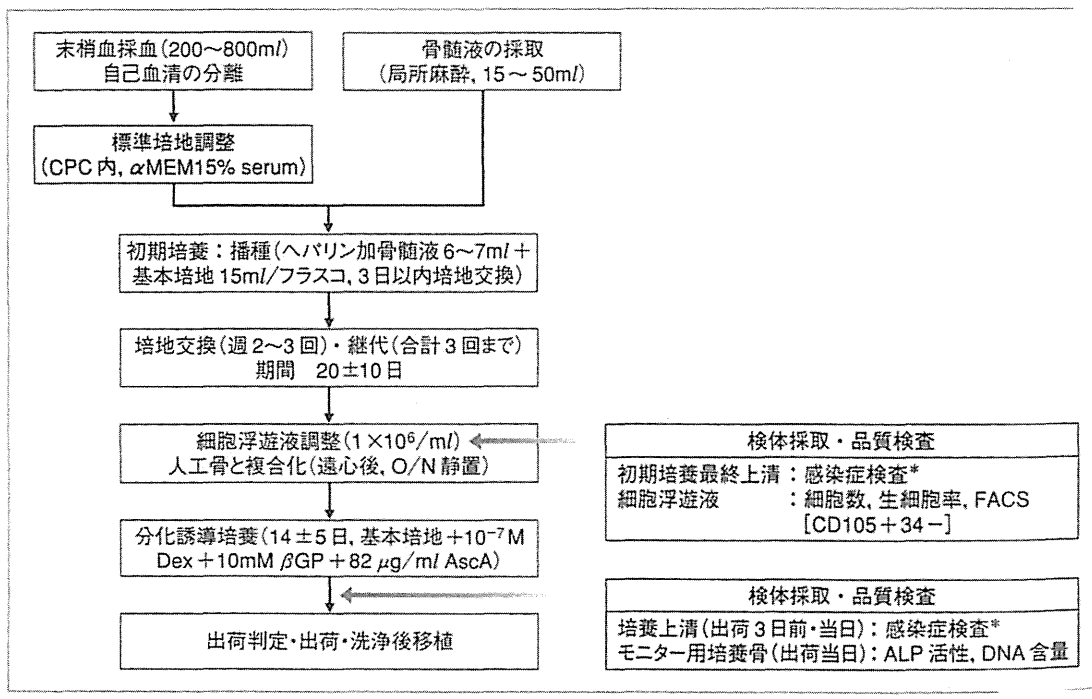

図2　自家骨髄由来培養細胞導入人工骨の製造工程

培養は基本培地の調整からすべてヒト移植用細胞専用の細胞培養調製施設で行われる。総工程は34日程度を要する。品質検査を2回実施しその結果で出荷判定を行う（*感染症検査［無菌試験，マイコプラズマ，エンドトキシン］）。

する必要がある。一般に，がん領域の臨床試験において世界共通で用いられている有害事象共通用語規準(Common Terminology Criteria for Adverse Events；CTCAE)[3)7)]や，厚生労働省の『医薬品等の副作用の重篤度分類基準について』(平成4年6月29日 薬安第80号 厚生省薬務局安全課長通知)[3)8)]などが利用できる。CTCAEは米国National Cancer Institute（NCI）が作成した有害事象の重篤度分類で，現在，v4.0日本語訳JCOG版（略称：CTCAE v4.0-JCOG）が公開されており，日本臨床腫瘍研究グループ（Japan Clinical Oncology Group；JCOG）のホームページからダウンロードすることが可能である。これは日米欧医薬品規制ハーモナイゼーション国際会議（ICH）によって開発された世界共通の医学用語集MedDRAにも対応しており，国際的に通用するものとなっている。

われわれの臨床研究では，有害事象については，実際に培養骨の移植を受けた9症例を対象に評価した。本臨床研究を通じて，50件の有害事象が観察されたが，術後の局所感染や，新規の腫瘍形成は1例もなく，そのほか，臨床的に問題となる強い有害事象はなかった。有害事象の内訳として疼痛（8件），ヘモグロビン減少（6件）が多くみられた。次いで，低ナトリウム血症（4件），高ビリルビン血症（3件）が観察された。また，Grade 3以上の有害事象は観察されず，Grade 2の発現があった有害事象は高ビリルビン血症が2件，疼痛，便秘，発熱が各1件であった。経過観察期間終了後，1例で巨細胞腫の再発が確認されており，本治療法により再発が促進された可能性は否定できないため，今後も慎重に評価する必要があると考えている。

2）有効性の評価

骨の再生医療に関する標準的臨床評価法として確立されたものはなく，従来の人工骨移植術で得られた経験から，多角的な骨再生能の臨床的評価法を設定して検討を行った。具体的には，有効性の主要評価項目は単純X線による骨癒合評価(Grade 0：骨溶解，1：不変，2：軽度癒合，3：高度癒合)[12)]，副次的評価項目は，整形外科医による総合的画像評価（単純X線，CT，MRI），アルミステップによる簡易骨密度半定量法，二重エネルギーX線吸収測定法（dual-energy X-ray absorptiometry；DXA）による培養細胞導入人工骨移植部の骨密度定量，CT値，造影MRI，患肢機能評価（Musculoskeletal Tumor Society）[13)]，包括的QOL評価（SF-36，Japanese ver. 1.2）[11)]を採用した。以下，主要な項目について概説する。

a）単純X線によるグレード分類（図3）

日常の診療における骨折治療や自家骨移植，人工骨移植の場合と同様に，単純X線2方向などで経時的に観察し骨癒合の程度をGrade 0（骨溶解：移植部周辺のX線透過性の上昇），Grade 1（不変：移植部および移植部周辺のX線所見に変化がない），Grade 2（軽度癒合：移植部X線透過性の軽度低下および移植部/周囲骨間の骨透亮線の消失），Grade 3（高度癒合：移植部X線透過性の高度低下および人工骨顆粒間の境界消失）の4段階で判定する。骨欠損の修復のX線スコアリングシステムとして，Lane and Sandhu[15)]が提示したものがあるが，このシステムは偽関節や難治性骨折などに対する再生医療の評価が想定され，骨欠損部分の何%が新生骨によって置換されているか，骨折線の消失の程度，リモデリングの程度で判定するので，偽関節や分節状の骨欠損のモデルで細胞のみ移植する場合やゲル，ポリマー，コラーゲンスポンジなどX線透過性材料を用いる場合は，利用できる。われわれの臨床研究の場合，主として海綿骨部分の欠損を対象としセラミックス人工骨をscaffoldとして用いるので，移植直後から骨折線や欠損部はほぼなくなってしまうため，Lane and SandhuのX線スコアはなじまず，むしろ移植後の修復過程を，術直後に比べたその後の変化で評価する指標が望ましい。そこで本研究では，以前，セラミックス人工骨の臨床試験で評価基準として用いたグレード分類[12)]を骨再生の臨床試験でも使用した。

b）DXA法による培養骨移植部の骨密度定量

DXAは骨密度を定量する検査法で，エネルギーレベルの異なる2つのX線を検査対象に照射し，それぞれのエネルギーの組織による吸収率

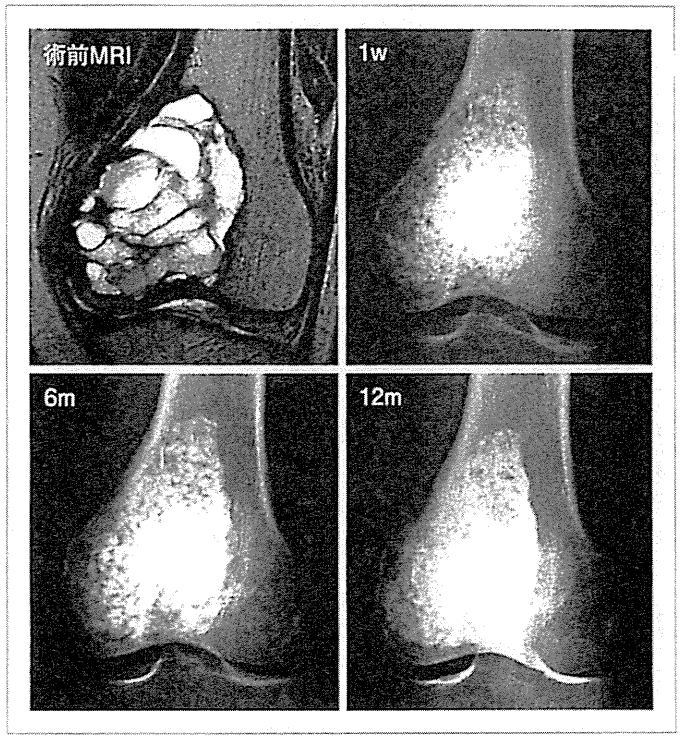

図 3　自家培養間葉系細胞導入人工骨による骨腫瘍切除後骨欠損の治療例
43 歳男性，左大腿骨骨巨細胞腫。初診時 MRI 所見（左上）と培養細胞導入人工骨移植後（1 週，6 カ月，12 カ月）の画像所見の変化。MRI では最大径 60 mm，推定骨欠損体積 52.4 cm^3 と大型の骨欠損であった。単純 X 線像の経時的変化では，培養骨移植術後 1 週（1 w）と比べて，術後 6 カ月（6 m）では移植部周辺部を中心に硬化像が見られる。軽度癒合（Grade 2）と判定した。術後 12 カ月では移植部の細胞導入人工骨の顆粒間の境界は消失し，全体として X 線透過性は著明に低下しており，高度癒合（Grade 3）と判定した。

の差異を利用して周囲の組織の影響をキャンセルし，検査対象部位の骨密度を正確に測定することができる。培養骨移植部位に region of interest (ROI) を設定することにより同部の骨密度を定量評価可能である。最近の全身用 DXA 装置では，任意の ROI を設定しその形状を解析用コンピュータに保存することができるので，特定部位の骨再生の程度を経時的に繰り返し評価するために適切な方法と考えられる。

c）造影 MRI

多孔体セラミックス人工骨など，X 線透過性の低いものを骨補填材として骨欠損部に埋植した場合，埋植部への生体組織，新生骨の侵入は単純 X 線像や CT での評価が困難である。多孔体セラミックス人工骨充填後の骨欠損部を造影 MRI で観察すると，人工骨埋植後早期から造影領域が周囲より出現し，経時的に深部へ進行することがわかっている。この造影領域の辺縁からの最大距離は，移植部に宿主側の循環系につながった血管組織が進入した深さを反映しているものと考えられる。直接骨新生を示しているわけではないが，骨再生には血管の新生が必須であることから重要な評価方法にもなり得ると考えられる。

d）機能および QOL 評価

経時的な患肢機能評価については，骨腫瘍手術後の患肢機能評価法として Musculoskeletal Tu-

mor Society の Functional Evaluation[13] が利用可能である。上肢用，下肢用に分かれているため，上下肢の比較をすることはできないが，病変の部位にかかわらず四肢機能の概要を簡便に評価できる指標であり，骨腫瘍の術後機能評価方法として国際的に広く利用されている。包括的 QOL 評価については，やはり国際的に広く用いられている SF-36™（MOS 36-Item Short-Form Health Survey）が利用できる。SF-36™ は，健康関連 QOL（HRQOL；health related quality of life）を測定するための，科学的で信頼性・妥当性を持つ尺度であり，運動器の手術前後の QOL 評価にも実績を持つ。現在，オリジナルの SF-36™（日本語版は version1.2）を改良した SF-36v2™ が標準版として使われている[14]。いずれのバージョンでも日本人の国民標準値が既に解析されているので，それを基準にして対象群の健康状態を検討することも可能である。

3. 骨再生医療臨床研究の結果と考察

われわれの臨床研究の有効性の評価の結果では，主要評価項目である単純 X 線像によるグレード分類において，移植後 48 週後での Grade 3 高度癒合の発現割合（66.7%，p=0.041）および Grade 2 以上の改善割合の経時的変化（8 週 44.4%，48 週 88.9%，p<0.001）はいずれも有意に改善していた。また副次評価項目のうち，DXA による骨塩定量，特に術後 1 週以内に実施した DXA による骨塩量を基準にその値の変化を経時的に見ると定量的に骨形成の程度が評価できるようである。この研究では，被験者ごとに一定の ROI の骨密度を経時的に測定したところ，移植直後の値に比べ，ほぼ全例で骨密度の上昇が観察された。最終観察時で骨塩量がやや低下した 1 例では，その後，骨巨細胞腫の再発が明らかとなっており，かなり鋭敏に骨再生の状況を反映できていると思われる。術直後のデータと比較した変化量を示すグラフは，定量的であることに加え，視覚的にも変化を捉えやすく有用な評価方法と考えられた。

患肢機能評価では，一部の症例で治療前の初期値が満点であり改善の程度を評価できないケースがあったが，多くの症例で経時的な数値の改善がみられており，有用な評価法と考えられる。一方，SF-36 の PCS（physical component summary：身体的健康度），MCS（mental component summary：精神的健康度）はともに，前観察時に比べ 48 週後では多くの症例で改善する傾向がみられたが，一方で低下する症例もみられ，全体としては改善傾向が認められるものの有意差は認められなかった。

このほか，総合的画像評価では全例で骨欠損が修復と判定されていた。造影 MRI 検査における造影領域の辺縁からの最大距離は，すべての症例で経時的に増加，すなわち造影範囲の拡大が確認された。一方，アルミステップによる簡易骨密度半定量法，最大割面での CT 値などは経時的な変化をうまく捉えることはできなかった。これらの測定値はいずれも基準値となる術後 1 週のデータが患部周囲の浮腫や出血などの影響で高値を示している可能性があり，そのため，その後の骨形成を鋭敏に捉えにくかったのではないかと考えている。信州大学で行われている「青壮年者の四肢良性骨腫瘍および骨腫瘍類似疾患掻爬後の骨欠損に対する β-リン酸三カルシウムを担体としたヒト培養自己骨髄間葉系細胞移植による骨欠損修復研究」では CT 横断面で移植部の CT 値×断面積を求め，各スライスの CT 値総和を体積で割った値，すなわち移植部全体の CT 値の平均を評価指標として用いており，評価指標として有効かどうか，結果が待たれる。このほか，骨シンチ SPECT（single photon emission computed tomography：単光子放射線コンピュータ断層撮影法）や ^{18}F-PET（positron emission tomography：陽電子放出型断層撮影法）などの核医学検査も骨再生を非侵襲的に，かつ生物学的に評価する方法として有用である可能性がある。

本研究では培養骨の作成過程や出荷時の品質管理として，いくつかの定量的な性能検査を行っているが，これらのパラメータと臨床評価のデータの相関をみると，培養骨出荷時のアルカリフォスファターゼ活性と術後の DXA の変化量に正の相関がみられた。本研究は対象症例が少なく引き続

き検討が必要であるものの，培養骨出荷時のアルカリフォスファターゼ活性は，個々の患者における培養骨の効果を予測する指標として重要である可能性がある。

われわれの培養骨による骨再生療法臨床研究の結果を総合すると，安全性に重大な問題はなく，目的とする骨欠損の修復が可能であるという意味で有効性も確認されたが，従来の自家骨移植や人工骨との比較はできていないので，今後は従来の治療法に対する優位性を検討する必要がある。本研究は骨再生に関するわれわれの最初の前向き研究として，良性骨腫瘍を対象に実施したが，今後，従来の治療法に対する優位性を臨床的に示すためには，悪性腫瘍切除後の大型骨欠損など，より難治性の骨欠損を対象にその有用性を検討していく必要があると考えている。

Ⅳ. 細胞を用いた骨再生医療の実用化の動向

このような細胞製品を用いた骨の再生医療は，まだ始まったばかりであり，臨床での安全性，有効性を客観的に評価した報告はこれまでわずかしかないが[15]，少数例のパイロット的臨床研究や臨床経験はとしては，われわれの方法と同様の ceramics scaffold と間葉系幹細胞を組み合わせた方法を含む種々の形の骨再生医療の試みが国内外から報告されており[1)~6)]，粉砕骨折や腫瘍による大型骨欠損に対して良好な修復が得られている。このような幹細胞と ceramics scaffold を用いた骨形成の促進技術は，骨再生医療としての臨床応用に加え，脊椎の固定術での骨移植の代替材料としても臨床例が報告されている。産業化という意味では現在のところ，国内外共に細胞とセラミックス人工骨を用いた骨再生の技術について製品化に至ったものはないが，細胞治療による骨再生としては海外では脊椎固定の目的で同種間葉系幹細胞（Osteocel™，NuVasive 社）が米国で製造販売承認が得られているほか，韓国では自家間葉系幹細胞由来骨芽細胞が偽関節，骨壊死や骨欠損の治療目的に実用化されている[16]。

文　献

1) Myoui A et al：A prospective clinical study to evaluate the safety and efficacy of autologous marrow-derived mesenchymal cells integrated with porous ceramic scaffold for bone defect after bone tumor removal. Final program, 10th Annual Meeting of the International Society for Stem Cell Research, 67, 2012
2) Quarto R et al：Repair of large bone defects with the use of autologous bone marrow stromal cells. N Engl J Med **344**：385—386, 2001
3) Vacanti CA et al：Replacement of an avulsed phalanx with tissue-engineered bone. N Engl J Med **344**：1511—1514, 2001
4) Morishita T et al：Tissue engineering approach to the treatment of bone tumors；three cases of cultured bone grafts derived from patients' mesenchymal stem cells. Artif Organs **30**：115—118, 2006
5) Kawate K et al：Tissue-engineered approach for the treatment of steroid-induced osteonecrosis of the femoral head：transplantation of autologous mesenchymal stem cells cultured with beta-tricalcium phosphate ceramics and free vascularized fibula. Artif Organs **30**：960—962, 2006
6) Marcacci M et al：Stem cells associated with macroporous bioceramics for long bone repair；6- to 7-year outcome of a pilot clinical study. Tissue Eng **13**：947—955, 2007
7) Dominici M et al：Minimal criteria for defining multipotent mesenchymal stromal cells；the International Society for Cellular Therapy position statement. Cytotherapy **8**：315—317, 2006
8) Nishikawa M et al：Bone tissue engineering using novel interconnected porous hydroxyapatite ceramics combined with marrow mesenchymal cells；quantitative and three-dimensional image analysis/ceramic construct；comparison with marrow mesenchymal cell/ceramic composite. Cell Transplant **13**：367—376, 2004
9) Sakamoto M et al：Development of superporous hydroxyapatites and their examination with a culture of primary rat osteoblasts. J Biomed Mater Res **82-A**：238—242, 2007
10) Hattori H et al：Bone formation using human adipose tissue-derived stromal cells and a

biodegradable scaffold. J Biomed Mater Res B Appl Biomater **76-B** : 230—239, 2006
11) Szpalski C et al : Bone tissue engineering : current strategies and techniques, Part I : Scaffolds. Tissue Eng Part **18-B** : 246—257, 2006
12) Myoui A : Three-dimensionally engineered hydroxyapatite ceramics with interconnected pores as a bone substitute and tissue engineering scaffold. Biomaterials in Orthopedics (ed by Yaszemski MJ et al), Marcel Dekker, 287—300, 2003
13) Enneking WF et al : A system for the functional evaluation of reconstructive procedures after surgical treatment of tumors of the musculoskeletal system. Clin Orthop **286** : 241—246, 1993
14) 福原俊一 : MOS Short-Form 36-Item Health Survey—新しい患者立脚型健康指標. 厚生の指標 **46** : 40—45, 1999
15) Lane JM et al : Current approaches to experimental bone grafting. Orthop Clin North Am **18** : 213—225, 1987
16) Kim SJ et al : A multi-center, randomized, clinical study to compare the effect and safety of autologous cultured osteoblast (Ossron) injection to treat fractures. BMC Musculoskelet Disord **10** : 20, 2009

* * *

* *

Impact of cardiac support device combined with slow-release prostacyclin agonist in a canine ischemic cardiomyopathy model

Yasuhiko Kubota, MD,[a] Shigeru Miyagawa, MD, PhD,[a] Satsuki Fukushima, MD, PhD,[a] Atsuhiro Saito, PhD,[a] Hiroshi Watabe, PhD,[b] Takashi Daimon, PhD,[c] Yoshiki Sakai, PhD,[a] Toshiaki Akita, MD, PhD,[d] and Yoshiki Sawa, MD, PhD[a]

Background: The cardiac support device supports the heart and mechanically reduces left ventricular (LV) diastolic wall stress. Although it has been shown to halt LV remodeling in dilated cardiomyopathy, its therapeutic efficacy is limited by its lack of biological effects. In contrast, the slow-release synthetic prostacyclin agonist ONO-1301 enhances reversal of LV remodeling through biological mechanisms such as angiogenesis and attenuation of fibrosis. We therefore hypothesized that ONO-1301 plus a cardiac support device might be beneficial for the treatment of ischemic cardiomyopathy.

Methods: Twenty-four dogs with induced anterior wall infarction were assigned randomly to 1 of 4 groups at 1 week postinfarction as follows: cardiac support device alone, cardiac support device plus ONO-1301 (hybrid therapy), ONO-1301 alone, or sham control.

Results: At 8 weeks post-infarction, LV wall stress was reduced significantly in the hybrid therapy group compared with the other groups. Myocardial blood flow, measured by positron emission tomography, and vascular density were significantly higher in the hybrid therapy group compared with the cardiac support device alone and sham groups. The hybrid therapy group also showed the least interstitial fibrosis, the greatest recovery of LV systolic and diastolic functions, assessed by multidetector computed tomography and cardiac catheterization, and the lowest plasma N-terminal pro-B-type natriuretic peptide levels ($P < .05$).

Conclusions: The combination of a cardiac support device and the prostacyclin agonist ONO-1301 elicited a greater reversal of LV remodeling than either treatment alone, suggesting the potential of this hybrid therapy for the clinical treatment of ischemia-induced heart failure. (J Thorac Cardiovasc Surg 2014;147:1081-7)

Left ventricular (LV) remodeling in ischemic and nonischemic dilated cardiomyopathy is characterized by progressive dilatation and dysfunction of the left ventricle, leading to severe heart failure.[1,2] The cardiac support device is a mesh net designed to reduce diastolic ventricular wall stress by mechanical means and thus prevent LV dilatation. It has been shown to halt LV remodeling in dilated cardiomyopathy in preclinical studies.[3-5] Clinical trials undertaken on the basis of these favorable results showed beneficial effects on LV remodeling, including significantly decreased LV end-systolic (LVESV) and end-diastolic volumes (LVEDV), and a significant improvement in New York Heart Association functional class.[6-8] However, despite these positive effects, the device has not been associated with reductions in mortality and has not been approved for clinical use.[9]

The synthetic prostacyclin agonist ONO-1301 acts as a myocardial regenerative biological drug to enhance reversal of LV remodeling.[10-12] The beneficial effects of ONO-1301 on the heart are mediated by up-regulation of angiogenic and antifibrotic molecules, such as hepatocyte growth factor (HGF), vascular endothelial growth factor (VEGF), and stromal cell–derived factor-1 (SDF-1).[10-12] This mechanism has been shown to result in the active suppression of ischemic and fibrotic changes in the myocardium.[10-12]

We hypothesized that the biological effects of the slow-release form of the synthetic prostacyclin agonist ONO-1301 might complement the mechanical effects of the cardiac support device, thus enhancing its therapeutic effects in ischemic cardiomyopathy.

MATERIALS AND METHODS

All animals used in this study received care in compliance with the Guide for the Care and Use of Laboratory Animals (National Institutes of Health publication no. 85-23, revised 1996).

Animal Treatment

A total of 28 beagles (Oriental Yeast, Co, Ltd, Tokyo, Japan) weighing 9 to 11 kg were used. General anesthesia was administered with intramuscular ketamine (10 mg/kg) and intravenous propofol (5 mg/kg) for induction,

From the Department of Cardiovascular Surgery,[a] Department of Molecular Imaging in Medicine,[b] Osaka University Graduate School of Medicine, Osaka, Japan; Department of Biostatistics,[c] Hyogo College of Medicine, Hyogo, Japan; Department of Cardiovascular Surgery,[d] Kanazawa Medical University, Ishikawa, Japan.

Supported by the New Energy and Industrial Technology Organization and the Japan Society for the Promotion of Science Core-to-Core Program.

Disclosures: Authors have nothing to disclose with regard to commercial support.

Received for publication Feb 12, 2013; revisions received May 9, 2013; accepted for publication May 16, 2013; available ahead of print Oct 15, 2013.

Address for reprints: Yoshiki Sawa, MD, PhD, Department of Cardiovascular Surgery, Osaka University Graduate School of Medicine, 565-0871, 2-2 Yamadaoka, Suita, Osaka, Japan (E-mail: sawa-p@surg1.med.osaka-u.ac.jp).

0022-5223/$36.00

http://dx.doi.org/10.1016/j.jtcvs.2013.05.035

Abbreviations and Acronyms

ANOVA	= analysis of variance
dp/dt	= delta pressure/delta time
Ees	= end-systolic elastance
HGF	= hepatocyte growth factor
LV	= left ventricular
LVEDV	= left ventricular end-diastolic volume
LVESV	= left ventricular end-systolic volume
MDCT	= multidetector computed tomography
MI	= myocardial infarction
NT-proBNP	= amino-terminal pro-brain natriuretic peptide
SDF-1	= stromal cell–derived factor-1
VEGF	= vascular endothelial growth factor

and inhaled sevoflurane (1%–2%) for subsequent maintenance, with endotracheal intubation and mechanical ventilator support. After completion of the experiments, the animals were killed under general anesthesia, using an overdose of intravenous sodium pentobarbital (18 mg/kg) to achieve complete sedation, followed by administration of an intravenous potassium-based solution.

Myocardial Infarction Induction

With the animals under general anesthesia, a minimal left thoracotomy was performed through the fifth intercostal space, and the heart was exposed by pericardiotomy. The left descending artery and diagonal vessels were ligated both proximally and distally using 5-0 polypropylene sutures to produce an anterior myocardial infarction (MI). Akinesis of the anterior wall was confirmed by epicardial echocardiography and the chest was closed in layers. The animals were allowed to recover.

Cardiac Support Device

The cardiac support device (0.9–1.0 g), made from polyglycolic acid (Nipro Corporation, Osaka, Japan), was designed on the basis of data obtained from multidetector computed tomography (MDCT) and a heart excised at 1 week postinfarction.

Treatments

The animals were assigned randomly to 1 of 4 groups at 1 week after infarct induction as follows: cardiac support device alone, cardiac support device plus ONO-1301 (hybrid therapy), ONO-1301 alone, or sham control group. In the cardiac support device alone group, 2 sheets of atelocollagen (50 × 50 mm) (Integran; Nippon Zoki Pharmaceutical Co, Ltd, Osaka, Japan) immersed in suspended polylactic and glycolic acid (10 mg/kg) were fixed on the whole surface of the ventricles and the cardiac support device was placed as described previously.[3-5] The same procedure was used in the hybrid therapy group, with the addition of ONO-1301[10-12] (10 mg/kg) (ONO Pharmaceutical Co, Ltd, Osaka, Japan) instead of the polylactic and glycolic acid. In the ONO-1301 alone group, 2 sheets of atelocollagen (50 × 50 mm) immersed in suspended ONO-1301 (10 mg/kg) were fixed on the whole surface of the ventricles. The sham group was subjected to the same procedures as the ONO-1301 alone group, except for the use of polylactic and glycolic acid instead of ONO-1301.

Transthoracic Echocardiography

Transthoracic echocardiography was performed using a 5.0-MHz transducer (Altida; Toshiba Medical Systems Corporation, Tochigi, Japan) for 2-dimensional speckle-tracking echocardiography under general anesthesia. The data were analyzed using 2-dimensional Wall Motion Tracking software (Toshiba Medical Systems Corporation) as previously described.[13]

MDCT

Electrocardiography-gated MDCT was performed using a 16-row MDCT scanner (SOMATOM Emotion 16-Slice Configuration; Siemens, Munich, Germany) during an end-expiratory breath-hold under general anesthesia. MDCT was performed after intravenous injection of 30 mL of nonionic contrast medium (Iomeron; Bracco, Milan, Italy). All images were analyzed on a workstation (AZE VirtualPlace Lexus64; AZE, Tokyo, Japan). LVEDV and LVESV, LV ejection fraction, LV end-diastolic and end-systolic sphericity indices, and LV/right ventricular end-diastolic and end-systolic diameter values were obtained from the workstation.

Cardiac Catheterization

Under general anesthesia, a 3F micromanometer-tipped catheter (SPR-249; Millar Instruments, Houston, Tex) was inserted through the ventricular apex via a left thoracotomy to measure hemodynamic parameters and cardiac functions, including end-systolic pressure and end-diastolic pressure, delta pressure/delta time (dp/dt) maximum, dp/dt minimum, end-systolic elastance (Ees), and the time constant of relaxation in the left and right ventricles. LV volume was altered by occluding the inferior vena cava with tape via a left thoracotomy.

Wall Stress Calculation

LV wall stress was evaluated using specifically developed software (YD, Ltd, Tokyo, Japan) on an off-line personal computer. Global end-systolic and end-diastolic wall stresses were calculated on the basis of the data obtained from MDCT and cardiac catheterization.[14]

Cardiac Positron Emission Tomography

^{13}N-ammonia (200–300 MBq) positron emission tomography (PET) was performed using a HeadtomeV/SET2400W (Shimadzu, Co, Kyoto, Japan) under general anesthesia. Myocardial blood flow was quantitated using PMOD software (version 3.2) (PMOD Technologies, Ltd, Zurich, Switzerland) and divided into 17 segments as recommended by the American Heart Association.

Histologic Analysis

Paraffin-embedded transverse sections of the excised hearts were stained with periodic acid-Schiff to measure the short-axis diameter of the myocytes, and with Masson trichrome to assess the extent of fibrosis. The sections were immunostained with anti-CD31 antibody in LSAB kits (DakoCytomation, Glostrup, Denmark). Myocyte diameters and vascular density were measured in 10 different randomly selected fields using a Biorevo BZ-9000 fluorescence microscope (Keyence, Osaka, Japan), and percentage fibrosis was calculated using MetaMorph software (Molecular Devices, Tokyo, Japan).

Real-Time Polymerase Chain Reaction

Total RNA extracted from cardiac tissue was reverse-transcribed using TaqMan reverse transcription reagents (Applied Biosystems, Foster City, Calif), and assayed using the ABI PRISM 7700 (Applied Biosystems). The average copy number of gene transcripts was normalized to that of glyceraldehyde 3-phosphate dehydrogenase for each sample.

Statistical Analysis

All statistical analyses were performed using JMP software (JMP9; SAS institute, Inc, Cary, NC). Results are presented as the mean ± standard deviation. Cardiac catheterization and histologic data were compared by 1-way analysis of variance (ANOVA). MDCT, echocardiography, wall stress, and amino-terminal pro-brain natriuretic peptide (NT-proBNP)

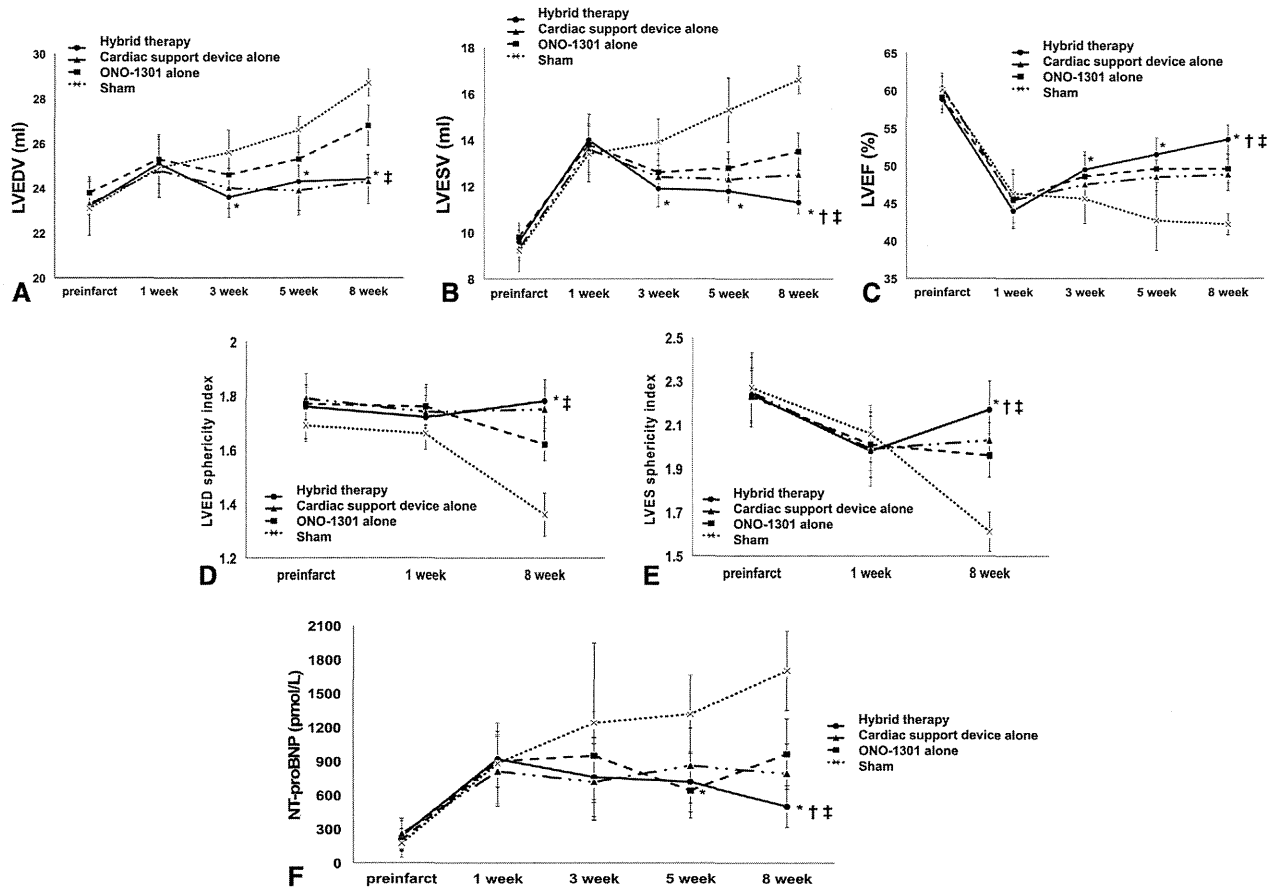

FIGURE 1. MDCT analysis. A, Changes in LVEDV. B, Changes in LVESV. C, Changes in LV ejection fraction. D, Changes in left ventricular end-diastolic and, (E) end-systolic sphericity indices. F, Changes in NT-proBNP. Hybrid therapy is shown by *circles with a solid line*, a cardiac support device alone is shown by *triangles with a dashed/dotted line*, ONO-1301 alone is shown by *squares with a dashed line*, and sham is shown by *crosses with a dotted line*. $*P < .05$ versus corresponding sham, $\dagger P < .05$ versus corresponding cardiac support device alone, $\ddagger P < .05$ versus corresponding ONO-1301 alone. *LV sphericity index*, LV long-axis diameter/LV short-axis diameter. *LVEDV*, Left ventricular end-diastolic volume; *LVESV*, left ventricular end-systolic volume; *NT-proBNP*, amino-terminal pro-brain natriuretic peptide.

data were compared by repeated ANOVA, using values obtained by subtracting the values at 1 week postinfarction from the values at each time point. Significant differences shown by ANOVA were subjected to post hoc analysis with Bonferroni correction. Sample size justification was not performed. A *P* value less than .05 was considered statistically significant.

RESULTS

Procedure-Related Morbidity and Mortality

Twenty-four animals completed the study. Three of the animals that failed to complete the study died within 1 week postinfarction and the remaining animal, which was a sham control, died at 7 weeks postinfarction. No dogs developed infections or had insufficient MI.

Recovery of Global Cardiac Performance With Hybrid Therapy

Global cardiac performance after the treatment was assessed serially and comprehensively by MDCT and cardiac catheterization. Both LVEDV and LVESV tended to increase after MI induction in the sham group (Figure 1, *A* and *B*). LVEDV was significantly smaller in the hybrid therapy group compared with the sham group at 3 and 5 weeks postinfarction, and significantly smaller than in both the ONO-1301 alone and sham groups at 8 weeks postinfarction. LVESV in the hybrid therapy group was significantly smaller than that in the sham group at 3 and 5 weeks, and was significantly smaller than that in the other groups at 8 weeks. As a result, LV ejection fraction was significantly greater in the hybrid therapy group compared with the sham group at 3 and 5 weeks, and significantly greater than in the other groups at 8 weeks (Figure 1, *C*).

The LV end-diastolic sphericity index was significantly greater in the hybrid therapy group compared with the ONO-1301 alone and sham groups at 8 weeks postinfarction (Figure 1, *D*). The LV end-systolic sphericity index decreased in all groups at 1 week postinfarction, whereas at 8 weeks the LV end-systolic sphericity index had decreased